Geophysical Journal International

Geophys. J. Int. (2010) **180,** 465–474 doi: 10.1111/j.1365-246X.2009.04400.x

Three-dimensional GPR imaging of the Benmore anticline and step-over of the Ostler Fault, South Island, New Zealand

Shamus C. Wallace,[1,*] David C. Nobes,[2,†] Kenneth J. Davis,[3] Douglas W. Burbank[4] and Antony White[5,§]

[1] *Formerly at Department of Geological Sciences, University of Canterbury, Christchurch, New Zealand*
[2] *Department of Geological Sciences, University of Canterbury, Private Bag 4800, Christchurch, New Zealand. E-mail: david.nobes@canterbury.ac.nz*
[3] *Formerly Institute for Crustal Studies and Department of Geological Sciences, University of California, Santa Barbara, CA 93106, USA*
[4] *Institute for Crustal Studies and Department of Geological Sciences, University of California, Santa Barbara, CA 93106, USA*
[5] *Formerly Flinders University, Adelaide, South Australia*

Accepted 2009 September 27. Received 2009 August 11; in original form 2007 November 7

GJI Geodynamics and tectonics

SUMMARY

Because surface processes can frequently remove, mask or suppress the surface expression of faults, geophysical imaging is needed to provide information on the geometric expression of the fault in the subsurface, including dips, the presence or absence of splays and folds and the nature of the material in the fault plane. Subsurface data become especially important where a step-over occurs, however the mechanism of the step-over is not clear. The Ostler Fault is a major thrust fault in the Mackenzie Basin of the South Island of New Zealand. The geometry of the fault changes along its length, with a number of growing anticlines and step-overs forming the Ostler Fault Zone (OFZ). One of these anticlines occurs along the Benmore segment of the OFZ. A three-dimensional (3-D) ground penetrating radar (GPR) survey was carried out to supplement detailed surface topographic mapping and help characterize the nature of the OFZ at Benmore. To cover the 1 km length of the step-over, the 3-D survey was done with a coarse yet regular 50 m line spacing. The individual fault splays were continuous and could be traced from line to line. Not all splays had surface expression, whereas almost all surface features had corresponding subsurface expression. As the fault approaches the anticline and multiple splays become apparent, the main fault simply develops into one of a set of splays as the deformation becomes distributed across the wider zone. Eventually, one of the other splays becomes the primary fault strand, and the others are abandoned.

Key words: Ground penetrating radar; Neotectonics; Folds and folding; Fractures and faults; New Zealand.

1 INTRODUCTION

Surface expressions of faults are subject to active processes that can reduce or even remove the fault exposure. Even active faults with apparently good surface expression can be incompletely exposed. Geophysical imaging, when combined with detailed global positioning satellite (GPS) topography, yields much additional information on the subsurface structure, including fault dips, the presence of splays and backthrusts, and the mapping of folds in the subsurface.

Ground penetrating radar (GPR) in particular has provided detailed imaging of small portions of both normal and thrust faults (Cai *et al.* 1996; Yetton & Nobes 1998; Chow *et al.* 2001; Gross *et al.* 2000, 2003), however generally over areas less than 1 ha in size. For the Benmore segment of the Ostler Fault zone (OFZ), we wanted to examine the change in the structural style over an area greater than 50 ha in size. The site also has gentle to moderate topography. GPR surveys have been successfully carried out over moderate to severe topographic relief before (e.g. Heincke *et al.* 2002), however again at scales of 10 s of m rather than 100 s of m.

The Ostler Fault in the Mackenzie District of the South Island of New Zealand (Fig. 1) is an active thrust fault system, over 50 km long, that accommodates approximately 7 per cent of the convergence between the Australian and Pacific plates east of the Southern Alps (Davis *et al*. 2005). The OFZ is segmented, and along the Benmore segment in particular, displacement between two non-overlapping fault segments is transferred through large-scale folding and an array of small faults. As Davis *et al.* (2005) note, the 'mapped surface ruptures do not presently overlap at the surface'. Thus, GPR imaging was complemented by detailed GPS topography, for the purpose of obtaining images of the evolution of these small faults and the growing anticline along the Benmore segment of the OFZ. The migrated GPR profiles allow us to determine the fault dips that are of the same order as those determined from the

*Now at: Tonkin and Taylor, Christchurch, New Zealand.
†Corresponding author.
§Deceased.

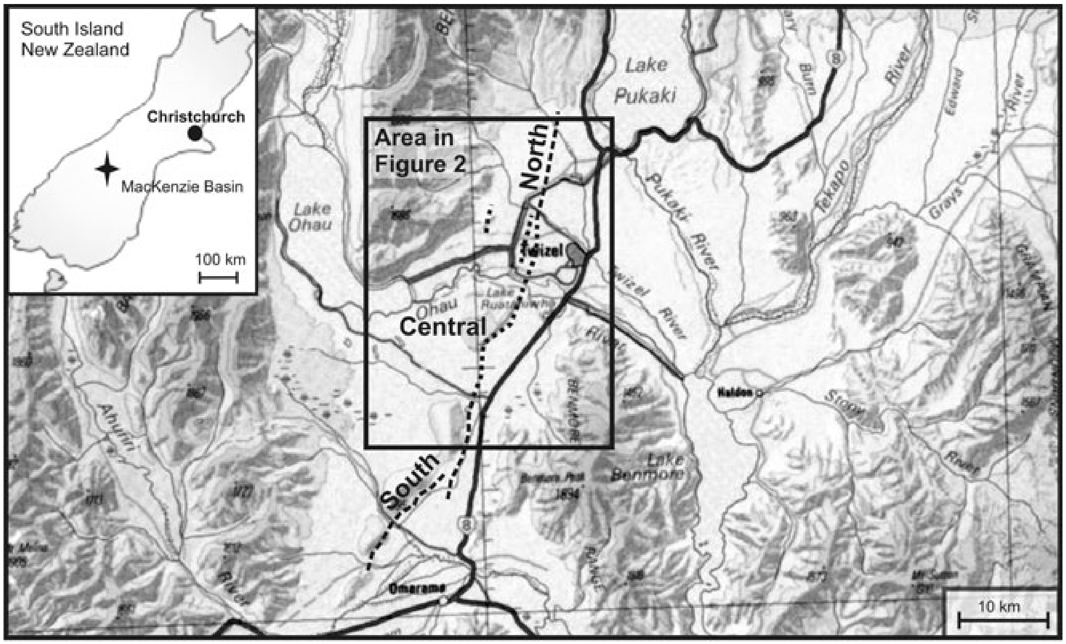

Figure 1. The Ostler Fault zone (OFZ) is a major structural feature in the Mackenzie Basin, which is located in the South Island of New Zealand (inset). The surface expression of the OFZ is shown dotted. The geology of a portion of the area (shown boxed) is shown in Fig. 2, which includes the study site. (Adapted from TopoMap NZ 2.0.)

sparse exposure of the fault in outcrop. The dips have been used to constrain the deformation of the OFZ (Amos *et al.* 2007).

Splays were traced to depths of more than 10 m, and splays were located that have little or no surface expression. In addition, the splays could be traced from profile to profile, allowing a general model of the shallow structure of the Benmore segment to be constructed.

2 GEOLOGY AND TECTONICS OF THE SITE

The surface trace of the OFZ extends in an approximately north–south trend along the western edge of the intermontane Mackenzie Basin. The basin itself is surrounded by peaks composed of Torlesse greywacke and Haast Schist, indurated Neogene sediments form the basin bedrock, and the basin is filled by significant thicknesses of poorly indurated glacial outwash sediments (Read 1984; Fox 1987; Blick *et al.* 1989) (Fig. 2).

The present basin morphology largely developed during four major Late Quaternary periods of glacial advance and retreat. The interior of the basin is generally of low relief associated with the multiple glacial outwash surfaces. The topography is limited to resistant pockets of bedrock that were not worn down by glaciers or transverse rivers. Hummocky ground, characteristic of the termini of retreating glaciers, is largely responsible for the damming of the three main glacial-derived lakes in the basin. The outwash surfaces create flat-lying terraces downstream (Fox 1987; Blick *et al.* 1989), which have been subsequently deformed by the Ostler Fault.

The OFZ lies to the east of the NNE-SSW trending Alpine Fault. Present motion of the Pacific Plate to the east relative to the Australian Plate to the west is approximately 45 mm yr^{-1}, oblique to the Alpine Fault (Blick *et al.* 1989; McClay 1992). Up to 40 mm yr^{-1} of the motion is parallel to the Alpine Fault, and is responsible for the primarily dextral strike-slip motion along the Alpine Fault;

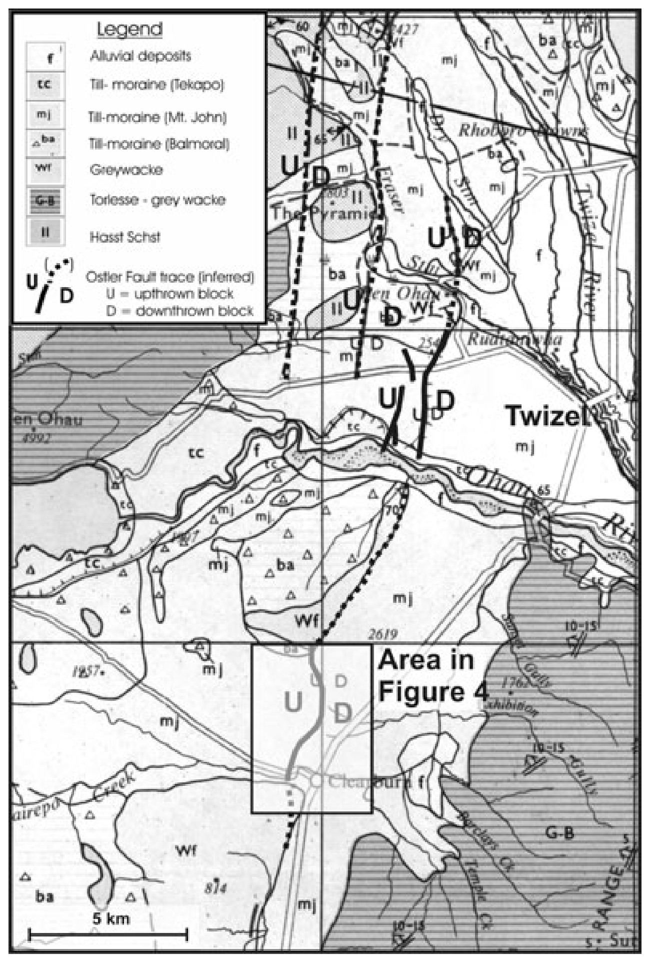

Figure 2. Geological map of the Twizel area, with the position and sense of motion of the Ostler Fault indicated. The location of the air photo of the study site (Fig. 4) is shown for reference. (Modified from Gair 1967.)

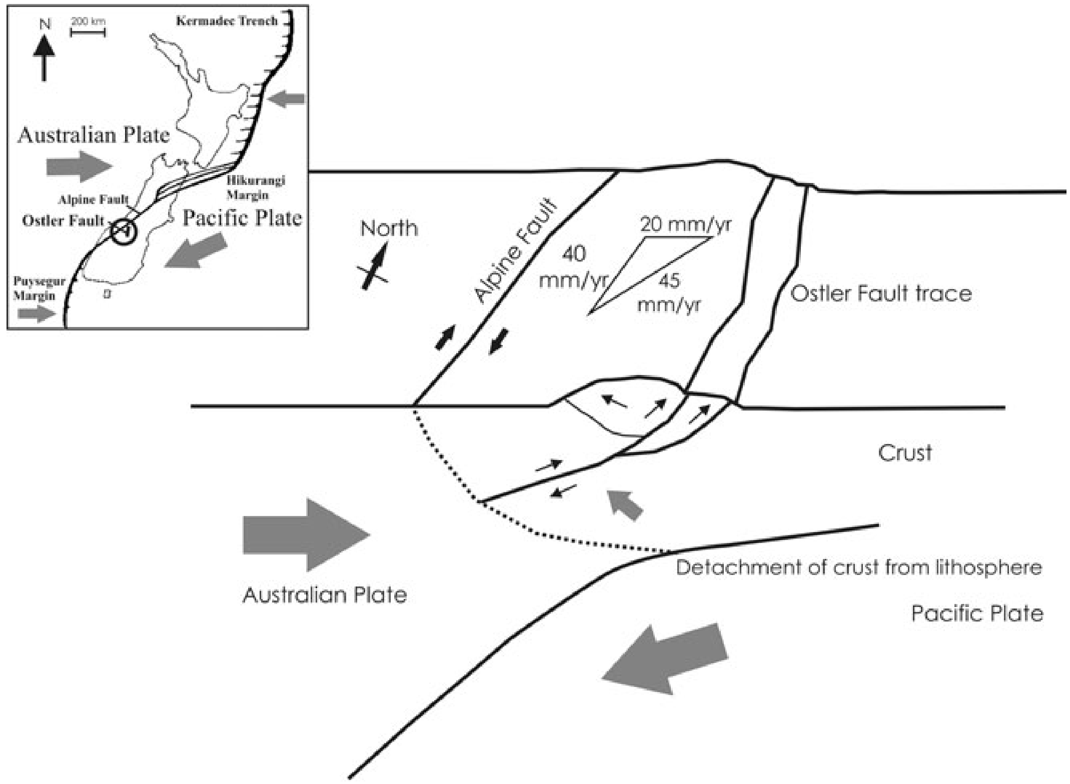

Figure 3. The geometry of the Ostler Fault is sketched in a perpective block diagram, in the context of its larger tectonic framework and its likely relationship with the Alpine Fault, which constitutes the major structural feature along the boundary between the Pacific and Australian plates (inset).

at least 20 mm yr^{-1} is normal to the Alpine Fault. Much of the compressional deformation is taken up along many faults to the east of the Alpine Fault (e.g. Blick *et al.* 1989; Long *et al*. 2003; Davis *et al*. 2002, 2005; Amos *et al*. 2007; Ghisetti *et al.* 2007), in particular along thrust faults such as the Ostler Fault (Fig. 3).

Deformation along the fault is not restricted to a single scarp, but is stretched over a zone approximately 3 km wide (Read 1984; Ghisetti *et al*. 2007). Commonly, individual scarps related to the surface rupture of the fault are not laterally continuous along the strike, and a number of step-over and exchange points occur between offset scarps. Changes both in the local strike and in the complexity of the surface exposure of the fault, as a single scarp or as multiple splays, are clear geomorphic features on the outwash surfaces (e.g. Read 1984; Davis *et al*. 2002, 2005; Amos *et al*. 2007). The OFZ can be divided into three sections, northern, central and southern, using the changing character along its length (Fig. 1). The central zone, located approximately between the Twizel River to the north and Wairepo Creek to the south, is unlike the northern and southern sections in that, for the most part, the central zone is characterized not by a single scarp but rather by multiple scarps and the westward tilting of the hanging wall fault blocks (Read 1984; Ghisetti *et al*. 2007). The 3-D radar survey focused on the southern end of the central segment, near Benmore, where a hangingwall anticline deforms the outwash surface. The fold occurs at a transfer zone from one main fault scarp to a series of small multiple scarps and then into another main fault that is offset from the first (Fig. 4). Fold height ranges from 5 to 20 m. Coincident with the fold is a series of small fault scarps, and where the fold height is greatest, the summed scarp displacement is least (Fig. 5; Davis *et al.* 2005).

3 METHODOLOGY

3.1 Ground penetrating radar

3.1.1 Basic principles

The principles of GPR have been well described elsewhere (e.g. Davis & Annan 1989; Daniels 1996), but GPR is still enough of a novelty that the basic concepts are briefly outlined here. GPR uses high-frequency electromagnetic signals (radio waves) directed into the ground. The transmitting antenna sends out a shaped pulse of high-frequency electromagnetic energy (Fig. 6). The receiving antenna sees three basic types of signals: a direct air wave, which travels at 300 m μs^{-1}; a direct ground wave, which travels at speeds of 40–200 m μs^{-1}, depending on the properties of the ground; and waves reflected from subsurface boundaries where the electric and dielectric physical properties change (Fig. 6a). The radar echoes returned to the surface thus yield information on subsurface layering and structure. The radar velocity in the ground depends on many factors, but is primarily controlled by the water content.

The direct and reflected radar energies are typically recorded as part of a shaded wiggle trace (Fig. 6b), much as is done for seismic traces. The direct air wave provides a convenient timing reference for the recorded traces. The time it takes for the signal to travel to a reflector and for the echo to return, the two-way traveltime (TWT), is dependent on the distance to the reflecting feature and on the radar velocity between the surface and the reflector. Successive traces are plotted next to each other, as a function of TWT and position, and the continuity of the subsurface reflections can be observed. Radar profiles are most commonly acquired in 'common

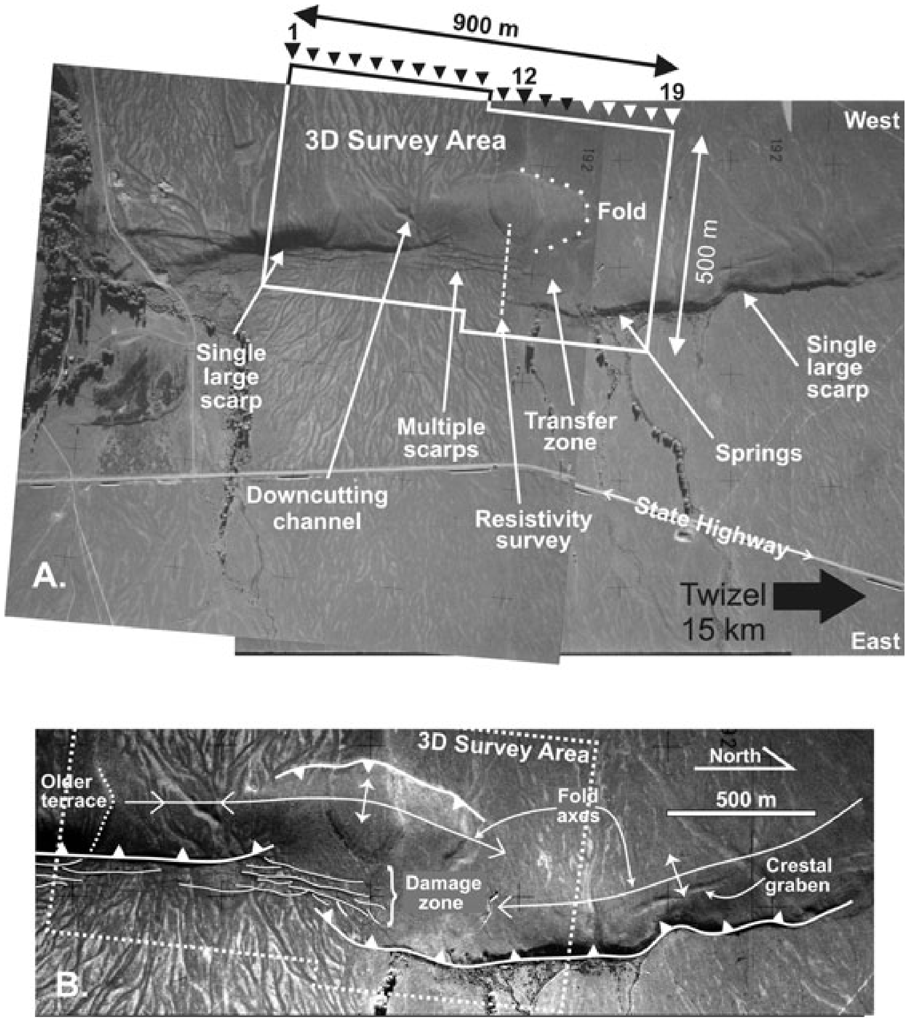

Figure 4. (a) Air photo of the Benmore segment of the OFZ, showing: the 3-D radar survey area (boxed), the location of a multi-electrode resistivity line and the major geomorphic and structural features present at Benmore. Note the developing fold, and the multiple small scarps that appear to be associated with the fold and with a step-over in the main fault scarp. (b) Structural geological features at Benmore site (from Davis *et al.* 2005).

offset' mode, the standard survey geometry where the transmitting and receiving antennas are kept at a fixed separation while the antenna pair is moved along at a constant pace or at constant steps between successive readings or traces. Frequently, the wiggle trace is removed, leaving only the variable area shading, and this is the display format used here.

An alternative survey format is a wide-angle reflection and refraction profile, which commonly uses a common midpoint (CMP) geometry (Fig. 7a). The resultant profile contains the direct air and ground waves and curved reflection events (Fig. 7b). The slope of the ground wave and the curvature of the reflection events yield subsurface velocity information, which is required for migration and time-to-depth conversion, as discussed in the next section. For the Benmore site, as for most of the OFZ, the subsurface radar velocity was found to be 90 m μs^{-1} (0.09 m ns^{-1}), characteristic of partly saturated sands and gravels.

3.1.2 Survey design and data processing

The Benmore GPR survey consisted of 19 lines, each approximately 600 m long and separated from the next nearest lines by 50 m (Fig. 4). The profiles were acquired in no specific order, but for ease of data entry and for continuity, the transects have been labelled 3D1 to 3D19, from south to north. The lines were oriented to cross the fault in an approximately perpendicular direction.

We used a Sensors & Software pulseEKKO^{TM} 100 system, with 50 MHz antennas mounted on a PVC trolley for ease of transport across the 50+ ha site. The parallel pair of antennas was oriented perpendicular to the survey direction, i.e. parallel to the strike of the fault. While using only one radar antenna orientation has been shown to be suboptimal (e.g. Lehmann *et al.* 2000), using antennas oriented parallel to the strike direction yields the maximum reflection energy from the fault and from the termination and truncation of beds by the fault (Nobes & Annan 2000).

The start and end of each line was pegged, and marker points were placed along each line, usually at the top of the anticline and at intervals on either side. Detailed topographic profiles were acquired using a Trimble 4700 differential GPS system, with cm-scale precision, both vertically and horizontally. The positions of all of the GPR survey markers were determined at the same time. The topography was later merged with the GPR profiles.

Only very basic processing of the radar data was needed. The GPR profiles were acquired in free-running continuous survey mode for speed and ease of data acquisition. Measuring tapes were hard to see at times, especially where the grass was long, but it was

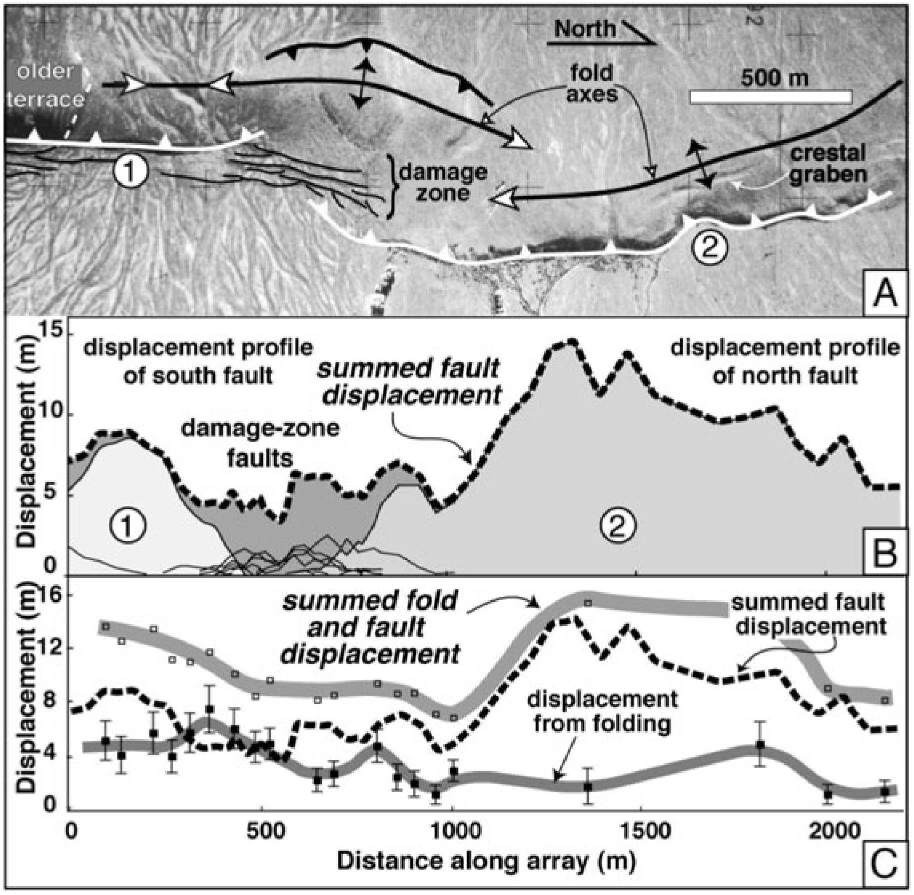

Figure 5. The apparent surface fault and fold displacement along the Benmore segment of the Ostler Fault (a) is distributed in folding and faulting (b) in such a way that the folding is greatest where the faulting appears to be least, and *vice versa* (c). Some of the discrepancy between northern, central and southern displacements may be taken up in subsurface faults with little or no surface expression. (Adapted from Davis *et al*. 2005.)

straightforward to tow the GPR trolley assembly at a relatively consistent pace. Some profiles were acquired in sections due to survey obstacles, or changing batteries in the midst of a profile, etc., and the sections were merged afterwards. The trace positions were then calculated using the locations determined from the GPS. The consistency of the survey speed could be checked by comparing the number of traces per profile segment. Then the traces were correctly positioned and resampled ('rubberbanded') to a constant separation. The average trace separation was 0.5 m, and this was the final trace spacing used for all profiles. The profiles were 'dewowed' to remove low-frequency 'noise' that is due to the saturation of the receiving antenna with time.

The final steps in processing were to carry out migration, to add topography to the profiles and to convert TWT to depth. Migration collapses diffraction (scattering) events to points and places dipping events in their proper, steeper, orientation (e.g. Yilmaz 2001). Migration and depth conversion require that we know the subsurface velocity. Hence, multiple CMP velocity surveys, as described earlier, were carried out at locations along the lines away from and parallel to the fault and fault splays. The structures thus had only minimal interference with the CMP profiles. The direct and reflected waves yielded velocities of 90 m μs^{-1} (0.09 m ns^{-1}), with little variation, and this velocity was then used for migration and depth conversion of the profiles.

The profiles were then interpreted via an iterative process. One profile would be interpreted, looking for such features as:

(1) water tables, generally locally perched, which would be relatively flat features that would cross stratigraphy;

(2) consistent breaks in bedding, bed truncations or sudden changes in bedding orientations, that would align with depth or time;

(3) rare reflections from faults, including back-thrusts and

(4) changes in bedding orientation with depth that was diagnostic of folding, where depth is a proxy for age.

The next profile would be interpreted, and the interpretation would be checked for consistency from one profile to the next. In this way, we could track the appearance and disappearance of splays, the growth of the folds along the anticline axis, etc. One sample profile (Line 3D19, a line from the northern end of the survey) is shown from raw to interpreted form in Fig. 8. Processed and interpreted profiles are also shown for Lines 3D12 (Fig. 9) and 3D1 (Fig. 10), which are representative of the central and southern parts, respectively, of the Benmore segment.

The profile interpretations have been done simply and conservatively. In some cases more could be made of the interpretation; for example, at the surface the fault dip can become shallow as it ramps towards the surface (Fig. 11), with associated colluvial wedges derived from loess and soil eroded from the steeper zones associated with the surface expressions of the fault splays. There are a number of such features that may be present in the profiles. However, the fault in the very near surface is not always clear because

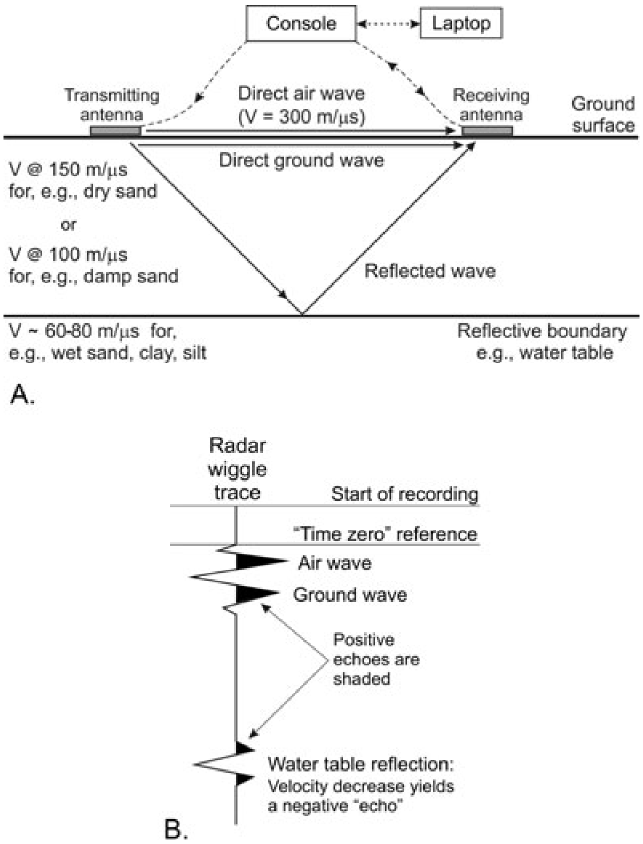

Figure 6. Basic principles of ground penetrating radar. (a) A pulse of radar energy is emitted from a transmitting antenna. The signal travels at the speed of light (300 m μs^{-1}) in air, but at a lower velocity in the ground depending on the subsurface materials. The receiving antenna records direct arrivals through the air and the ground, and echoes from subsurface boundaries. (b) The receiver records the radar echo strength as a function of two-way traveltime, and the trace is stored in the laptop. Successive traces are plotted side-by-side to yield a cross-sectional profile. (From Field *et al*. 2001.)

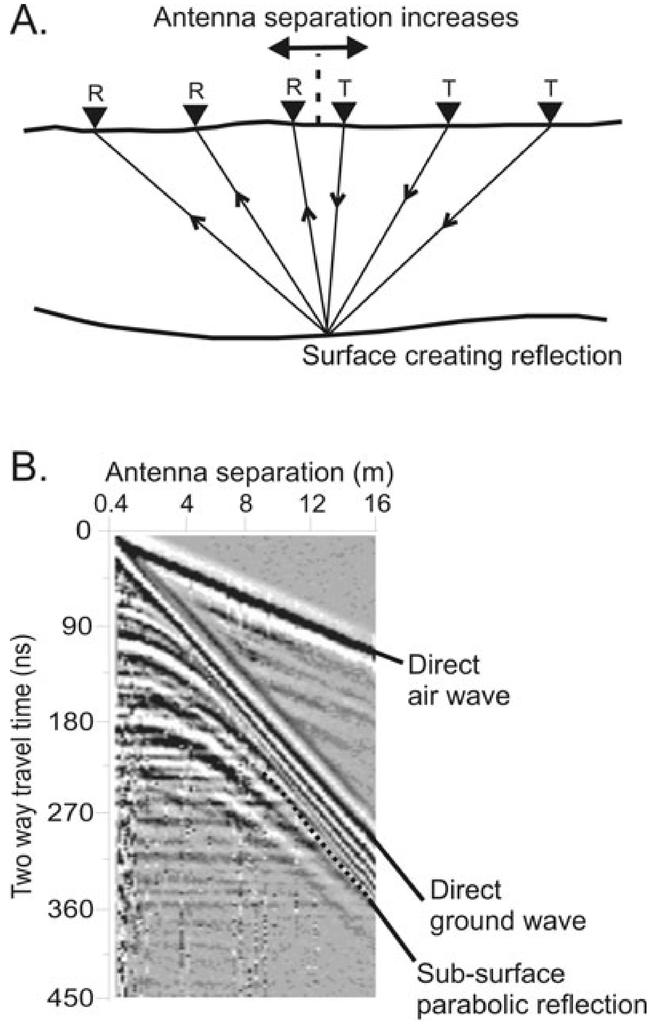

Figure 7. (a) The velocity structure of the subsurface can be obtained using a common midpoint (CMP) geometry. (b) The resultant CMP profile, as shown, is used to determine the subsurface radar velocity, which in turn is used to migrate the GPR profiles and to convert two-way traveltime (TWT) to depth. The example shown here is for the Benmore segment, and yields an average velocity of 90 m μs^{-1} (0.09 m ns^{-1}).

as its dip shallows, the fault expression can become confused with undulations in bedding, the remnants of erosional features (both current and relict), etc. The lack of trenching also limits the calibration of our interpretations. Thus, we have chosen to do the simplest, most direct interpretation of obvious bed truncations and displacements, which are mostly restricted to intermediate GPR depths.

4 RESULTS AND DISCUSSION

4.1 Representative GPR profiles

The appearance, evolution and disappearance of the main subsurface features can be traced from profile to profile across the transitional zone, so we only need to show a subset of the profiles to illustrate those features. Three representative GPR profiles are shown: 3D19 (Fig. 8) from the northern end and 3D12 (Fig. 9) and 3D1 (Fig. 10) from the middle and southern ends of the 3D survey. All profiles are shown with topography included and using automatic gain control (AGC) gains. AGC amplifies the GPR profiles so that all reflections are of comparable amplitude; this mode of presentation particularly aids stratigraphic analysis (e.g. Nobes *et al*. 2001). In addition, the profiles are plotted both with and without the interpretation superimposed. The sample profiles allow the range of features observed in the radar profiles to be illustrated for the full extent of the survey and to highlight changes in fault morphology along strike. The sample profiles will be discussed from north to south, starting with 3D19.

Profile 3D19 (Figs 8b and c) is characteristic of the more northerly profiles. A perched water table intersects the ground surface, producing a spring at the scarp created by the fault rupture. The spring was clearly identified at the time of the fieldwork and the reflection that was created by the perched water table is also clearly defined on several successive radar profiles. This reflection does not appear to follow the fault plane to depth rather it extends as an approximately level surface cutting across other reflectors. A possible second perched water table is also inferred, but could not be confirmed. More than one fault splay is inferred from the offset reflectors identified in this profile. The topography shows good correlation with the subsurface data; the major scarp clearly relates to the significant fault characteristics identified. Features associated with the backthrust can be seen in the profile.

Profile 3D12 (Figs 9a and b) is characteristic of the central zone where a step-over or offset occurs in the fault scarp. The surface expression of the major scarps that continue to the north and to the

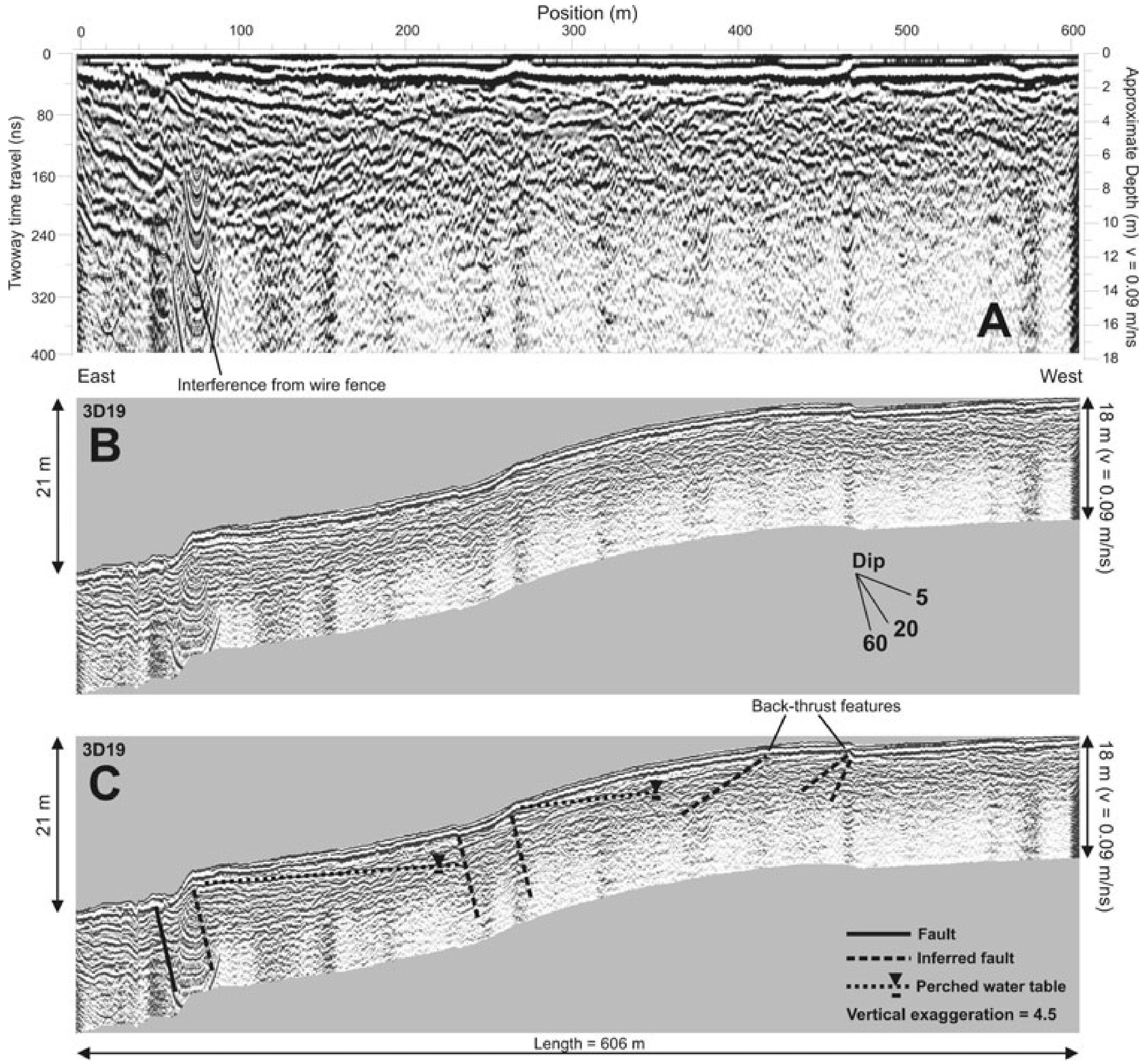

Figure 8. Profiles of the northernmost transect, 3D19, shown: (a) before processing and excluding any topographic correction; (b) fully processed including topography and (c) as in (b) but with the interpretation superimposed on the processed profile. Note the steep scarp and the perched water tables. Vertical exaggerations are approximate.

south of the central part of the site fade noticeably in the central area, to such an extent that they are hardly detectable in the central transects. The area between the two large offset scarps is characterized by the surface expression of multiple 'scarplets' and subsurface fault splays visible in the subsurface radar profiles. Significant features of the 3D12 profile include the identification of the multiple scarplets on the eastern side, whereas the topography and deformation of subsurface reflectors are evidence for the folding due to the fault deformation. The uppermost reflections that are consistent over the whole profile are recent sediments shed off the fault scarps that appear visible above the parallel units that drape the whole profile. These parallel units are interpreted as the youngest sediments that pre-date the onset of deformation after the abandonment of the outwash terrace. The surface expression of the fold is present in the deeper bed reflections, which were originally deposited approximately parallel to the surface of the time, and that now show a steepening of the dip with depth, indicating progressively more deformation of the deeper, older beds, as would be expected for ongoing folding. Also present in 3D12 and the other central Benmore transects is a small backthrust.

The southernmost profile, 3D1 (Figs 10a and b), is representative of the transects completed over the site south of the step-over zone and highlights the change in topographic distortion associated with the surface trace of the fault. The fault trace is highly pronounced with a distinctive scarp that correlates with the subsurface expression of the offset beds in the radar profile. Surface beds that follow the topography are again present while there is also some definition of the older beds at depth that show the gradual deformation due to folding. That the overlying beds dip less steeply is consistent with them being growth strata that were deposited as the fold was growing, but at a time when the rates of aggradation of the outwash surface outpaced the rate of vertical fold growth. The westward slope of the present fold limb can be seen in the gradual decrease in elevation of the right side of the profile.

The migrated TWT was used to determine the unexaggerated vertical extent. The traveltime (half of the TWT) was multiplied by

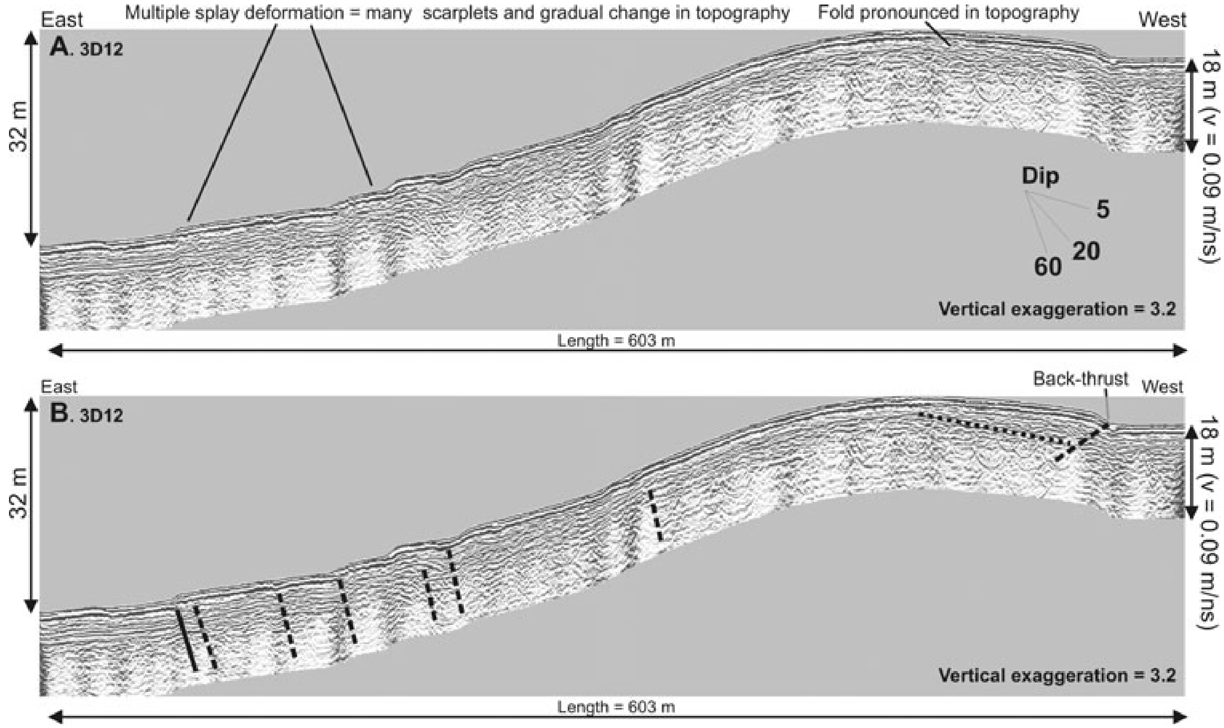

Figure 9. (a, top panel) 3D12 profile without interpretation superimposed. (b, bottom panel) Profile of transect 3D12 showing the multiple splays and the development of the fold associated with the offset in the line of strike of the main fault trace.

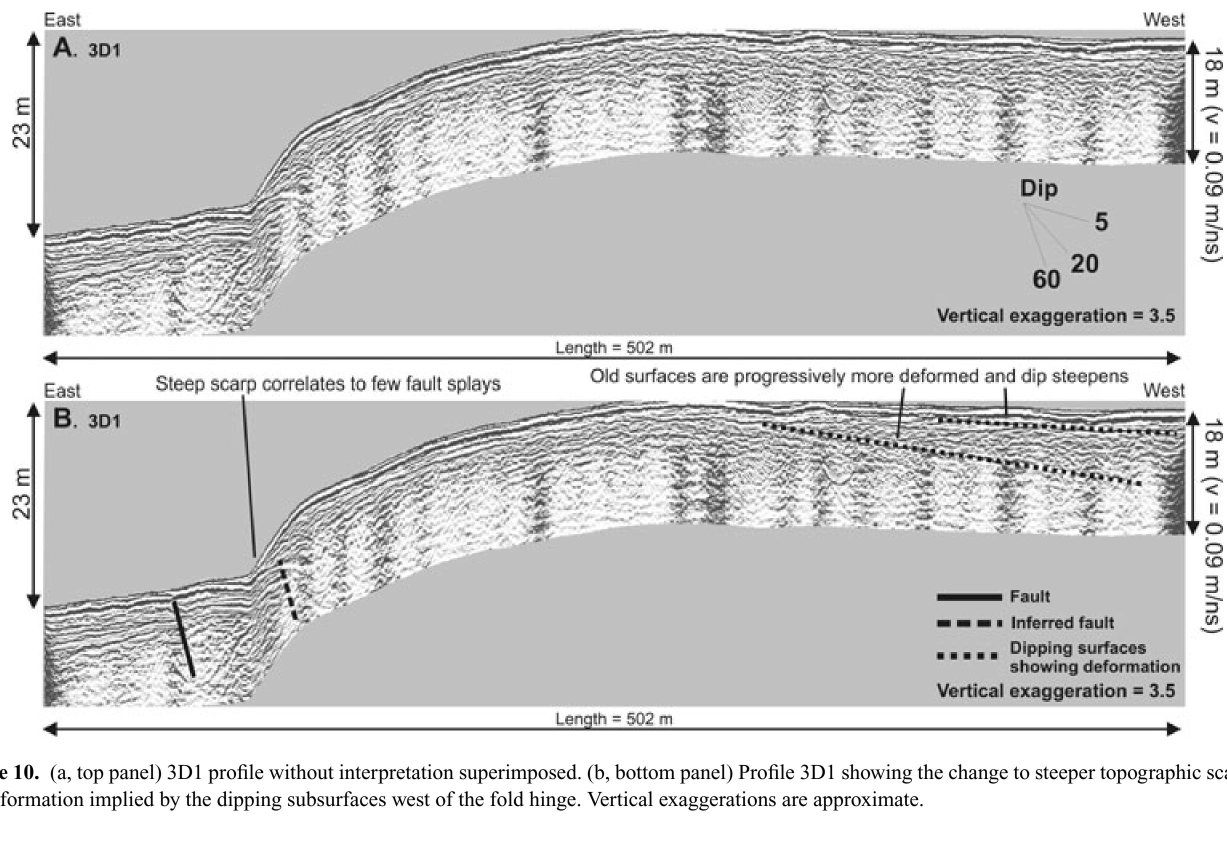

Figure 10. (a, top panel) 3D1 profile without interpretation superimposed. (b, bottom panel) Profile 3D1 showing the change to steeper topographic scarp and the deformation implied by the dipping subsurfaces west of the fold hinge. Vertical exaggerations are approximate.

the CMP velocity, in this case 0.09 m ns^{-1}, and the corresponding horizontal distance was then used to calculate the dip for the given fault splay. Dips were determined for the splays identified in the representative GPR profiles 3D1, 3D12 and 3D19; dips ranged from 46° to 59°. The mean dip was 51 ± 10° (2σ or 95 per cent confidence interval). These near-surface results are consistent with values obtained from seismic profiles up to 1.5 km in depth (Ghisetti *et al*. 2007).

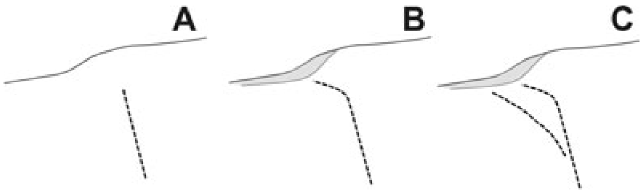

Figure 11. The simplest, most direct interpretation (a) has been used in Figs 8, 9 and 10. Alternative interpretations are possible, such as the dip becoming shallow as the fault ramps up to the surface (b) with an associated colluvial wedge (shaded), and a shallower dipping 'fault' that disturbs but does not truncate the beds (c).

4.2 3-D GPR interpretation

When the 2-D profiles are examined in 3-D, the structural relationships between the fault and fold features can be taken from the 2-D profiles into 3-D (Fig. 12). Characteristic features of displacement identified on the Benmore radar profiles are associated with multiple fault splay offsets, folding and thrusting. This includes the relationship between the step-over zone and the development of the fold in the southern and central section of the Benmore study area. A perched water table appeared as a highly distinctive reflector in the radar profiles and also issued from the ground as a spring adjacent to the base of the fault scarp, likely a result of a confining layer forced to the surface as a result of the faulting. The lateral extent of the water table can be identified in the 3-D image, dying out to the south, either due to the change in fault morphology, or more likely simply due to lack of water recharge or increased evapotranspiration in that area.

The fold is identified in both the aerial photos (Fig. 4) and the topographic surveys. Read (1984) and Davis *et al.* (2002, 2005) recognized westward tilting of the hanging wall block, which is also clearly visible in the GPR profiles; the dips of the sediment beds increase with depth of burial (Figs 10a and b and 12). Geomorphic features, including a downcutting drainage channel, also highlight the deformation. The folding increases south of the zone surrounding the major step-over, possibly as a secondary result of the step-over.

The 3-D image (Fig. 12) highlights the change in the nature of the fault, in both the surface and subsurface, over the site. The evolution in the morphology can be traced from profile to profile. The northern section has a distinctive singular scarp that is related to at most three subsurface fault traces. As our view of the profiles moves south, the effect of the step-over is highlighted with the identification of a number of multiple fault splays and scarplets and a backthrust that has developed as the hangingwall is thrust up in a small pop-up structure. The multiple fault splays in the step-over zone are likely a result of an increase in the area of deformation, perpendicular to the strike. Although almost all surface scarplets coincide with a corresponding subsurface deformation feature, the opposite of this is not true: some subsurface features have no corresponding surface expression (e.g. Figs 8b and c, 9a and b). The main fault from the north continues as one of the scarplets. Near the southern section, the fault again appears at the surface as a single scarp, which is the continuation of one of the scarplets; the other scarplets, including the continuation of the main fault from the northern end, cease to be active and most of the motion is concentrated in the single strand. The subsurface profiles suggest that some features are present at the foot of the scarp, possibly related to continuation of the splays along the strike.

5 CONCLUSIONS

The GPR investigations of the Benmore segment of the OFZ, when combined with detailed GPS topography, allow us to characterize the spatial evolution of the OFZ along the strike of the Benmore segment. Although the 2-D profiles allow a large amount of information to be obtained about the subsurface features of the fault, it is not until the profiles are aligned and a 3-D image is created that the significance of some of the features is recognized. Many features may appear to be minor or unrelated to each other in 2-D, but their correlation and continuity becomes clearer upon closer analysis of the sections in 3-D. Characteristic features of displacement associated with the complex nature of the fault morphology on the Benmore radar profiles are associated with multiple fault splay offsets, folding and thrusting. In particular, the main fault

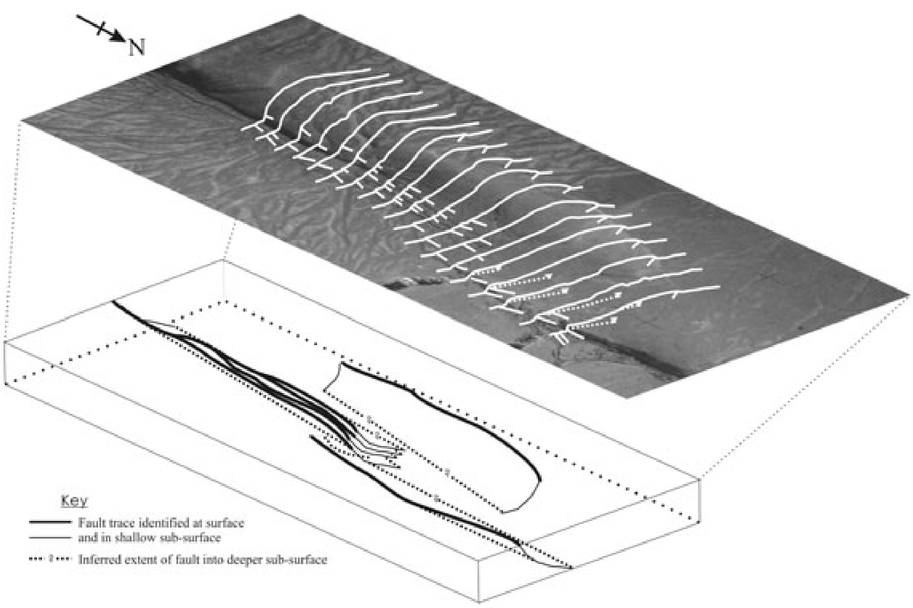

Figure 12. 3-D image generated from the collective interpretation of the 2-D GPR profiles. Each 2-D interpretation was related to adjacent profiles and the 3-D model was created. The subsurface interpretation shows strong correlation with the scarps and other features, such as channels at the surface.

continues as one of a number of splays as it enters the wider zone, so that although the faults at the surface do not appear to overlap, the subsurface imaging allows us to follow the continuity of the fault splays across the zone of the growing anticline. The total slip of distributed deformation is divided between the splays, only some of which are visible at the surface. At the other end of the wider zone, the deformation again becomes concentrated in fewer splays, until one splay takes over as the main fault trace.

ACKNOWLEDGMENTS

This research was part of a larger programme funded by the US National Science Foundation, under grant EAR-0117242.

REFERENCES

Amos, C.B., Burbank, D.W., Nobes, D.C. & Read, S.A.L., 2007. Geomorphic constraints on listric faulting: implications for active deformation in the Mackenzie Basin, South Island, New Zealand, *J. geophys. Res.,* **112**(B03S11), doi:10.1029/ 2006JB004291.

Blick, G.H., Read, S.A.L. & Hall, P.T., 1989. Deformation monitoring of the Ostler Fault Zone, South Island, New Zealand, *Tectonophysics,* **167,** 329–339.

Cai, J., McMechan, G.A. & Fisher, M.A., 1996. Application of ground-penetrating radar to investigation of near-surface fault properties in the San Francisco Bay region, *Bull. seism. Soc. Am.,* **86,** 1459–1476.

Chow, J., Angelier, J., Hua, J.J., Lee, J.C. & Sun, R., 2001. Paleoseismic event and active faulting: from ground penetrating radar and high resolution seismic reflection profiles across the Chishang Fault, eastern Taiwan, *Tectonophysics,* **333,** 241–259.

Daniels, D.J., 1996. *Surface-Penetrating Radar,* The Institution of Electrical Engineers, London, UK, 300 pp.

Davis, J.L. & Annan, A.P., 1989. Ground penetrating radar for high-resolution mapping of soil and stratigraphy, *Geophys. Prospect.,* **37,** 531–551.

Davis, K.J., Burbank, D.W., Wallace, S., Nobes, D.C. & Fisher, D., 2002. Variation of thrust-fault displacement and deformation style along segments of the Ostler fault zone, New Zealand, *EOS, Trans. Am. geophys. Un.,* **83**(47), American Geophysical Union Annual Fall Meeting, Supplement, Abstract T71B-1180.

Davis, K., Burbank, D.W., Fisher, D., Wallace, S. & Nobes, D., 2005. Thrust fault growth and segment linkage in the active Ostler Fault zone, New Zealand, *J. Struct. Geol.,* **27,** 1528–1546.

Field, G., Leonard, G. & Nobes, D.C., 2001. Where is Percy Rutherford's grave? in *Australian Connections and New Directions; Proc. Seventh Australian Archaeometry Conf.,* Vol. 5, pp. 131–147, eds Jones, M. & Sheppard, P., University of Auckland, Research in Anthropology and Linguistics.

Fox, A.N., 1987. The neotectonic history of the Lake Tekapo region, Mackenzie Basin, New Zealand, *MSc thesis* (unpublished). Department of Geology, University of Canterbury, Christchurch, New Zealand.

Gair, H.S., 1967. *Sheet 20, Mt. Cook (1st edn), Geological Map of New Zealand, 1:250 000,* Department of Scientific and Industrial Research, Wellington, New Zealand.

Ghisetti, F.C., Gorman, A.R. & Sibson, R.H., 2007. Surface breakthrough of a basement fault by repeated seismic slip episodes: The Ostler Fault, South Island, New Zealand. *Tectonics,* **26,** doi:10.1029/2007TC002146.

Gross, R., Hollinger, K., Green, A. & Begg, J., 2000. 3D ground-penetrating radar applied to paleoseismology: examples from the Wellington Fault, New Zealand, in *GPR 2000: Proc. Eighth Int. Conf. Ground Penetrating Radar,* SPIE Vol. 4084, pp. 479–481, eds Noon, D.A., Stickley, G.F. & Longstaff, D., SPIE, Bellingham, WA.

Gross, R., Green, A., Horstmeyer, H. & Holliger, K., 2003. 3-D georadar images of an active fault: efficient data acquisition, processing and interpretation strategies, *Subsurf. Sens. Technolog. appl.,* **4,** 19–40.

Heincke, B., Spillmann, T., Horstmeyer, H. & Green, A.G., 2002. 3-D georadar surveying in areas of moderate topographic relief, in *GPR 2002: Proc. Ninth Int. Conf. Ground Penetrating Radar,* SPIE Vol. 4758, pp. 223–227, eds Koppenjan, S.K. & Lee, H.L, SPIE, Bellingham, WA.

Lehmann, F., Boerner, D.E., Holliger, K. & Green, A.G., 2000. Multicomponent georadar data: some important implications for data acquisition and processing, *Geophysics,* **65,** 1542–1552.

Long, D., Cox, S.C., Bannister, S., Gersternberger, M.C. & Okaya, D., 2003. Upper crustal structure beneath the eastern Southern Alps and the Mackenzie Basin, New Zealand, derived from seismic reflection data. *N.Z.J. Geol. Geophys.,* **46,** 21–39.

McClay, J.R., 1992. *Thrust Tectonics,* Chapman and Hall, London, 447 pp.

Nobes, D.C. & Annan, A.P., 2000. "Broadside" versus "End-fire" radar response: some simple illustrative examples, in *GPR 2000: Proc. Eighth Int. Conf. Ground Penetrating Radar,* SPIE Vol. 4084, pp. 696–701, eds Noon, D.A., Stickley, G.F. & Longstaff, D., SPIE, Bellingham, WA.

Nobes, D.C., Ferguson, R.J. & Brierley, G.J., 2001. Ground-penetrating radar and sedimentological analysis of Holocene floodplains: insight from the Tuross valley, New South Wales, *Aus. J. Earth Sci.,* **48,** 347–355.

Read, S.A.L., 1984. The Ostler Fault Zone, in *Guidebook to the South Island Scientific Excursions International Symposium on Recent Crustal Movements of the Pacific Region, Royal Society of New Zealand Misc. Ser.,* Vol. 9, pp. 121–134, ed. Wood, P.R., Royal Society of New Zealand, Wellington.

Yetton, M.D. & Nobes, D.C., 1998. Recent vertical offset and near-surface structure of the Alpine Fault in Westland, New Zealand, from ground penetrating radar profiling, *N.Z.J. Geol. Geophys.,* **41,** 485–492.

Yilmaz, O., 2001. *Seismic Data Analysis: Processing, Inversion, and Interpretation of Seismic Data,* Society of Exploration Geophysicists, Tulsa, OK, 2027 pp.